Role of Hepatocyte RIPK1 in Maintaining Liver Homeostasis during Metabolic Challenges

Weigao Zhang[1], Danyang Zhang[1], Yuguo Yi[3], Liang Tao[4], Xunan Zhao[1], Qianchao Shao[1], Peiqi Li[1], Jianfa Zhang[1], Haibing Zhang[5*], Yuxin Chen[2*], Dan Weng[1*]

[1] *School of Environmental and Biological Engineering, Nanjing University of Science & Technology, 200 Xiaolingwei Street, Nanjing 210094, China*

[2]*Department of Laboratory Medicine, Nanjing Drum Tower Hospital, Nanjing University Medical School, Nanjing 210008, China*

[3]*School of medicine, Shenzhen Campus of Sun Yat-sen University, Sun Yat-sen University, Shenzhen 518107, China*

[4]*The First Affiliated Hospital, Basic Medical Sciences, University of South China, Hengyang 421001, China*

[5]*CAS Key Laboratory of Nutrition, Metabolism and Food Safety, Shanghai Institute of Nutrition and Health, Shanghai Institutes for Biological Sciences, University of Chinese Academy of Sciences, Shanghai 100864, China*

[*] **Correspondence**: **Dan Weng**, School of Environmental and Biological Engineering, Key Laboratory of Metabolic Engineering and Biosynthesis Technology, Ministry of Industry and Information Technology, Nanjing University of Science & Technology, 200 Xiaolingwei, Nanjing, China.

Tel: +862584318533; Fax: +862584318533.

Email: danweng@njust.edu.cn

Yuxin Chen, Department of Laboratory Medicine, Nanjing Drum Tower Hospital, Nanjing University Medical School, Nanjing 210008, China

Tel: +862568162671; Email: yuxin.chen@nju.edu.cn

Haibing Zhang, CAS Key Laboratory of Nutrition, Metabolism and Food Safety, Shanghai Institute of

Nutrition and Health, Shanghai Institutes for Biological Sciences, University of Chinese Academy of Sciences, Shanghai 100864, China

Email: hbzhang@sibs.ac.cn

Conflict of interest

The authors declare no conflict of interest with the contents of this article.

Abstract:

As a central hub for metabolism, the liver exhibits strong adaptability to maintain homeostasis in response to food fluctuations throughout evolution. However, the mechanisms governing this resilience remain incompletely understood. Receptor interacting protein kinase 1 (RIPK1) plays a key role in regulating cell survival, cell death, and inflammation. Despite extensive research on its involvement in various pathological conditions, the physiological role of RIPK1 remains relatively unexplored. In this study, we identified RIPK1 in hepatocytes as a critical regulator in preserving hepatic homeostasis during metabolic challenges, such as short-term fasting or high-fat dieting. Our results demonstrated that hepatocyte-specific deficiency of RIPK1 sensitized the liver to short-term fasting-induced liver injury and hepatocyte apoptosis in both male and female mice. Despite being a common physiological stressor that typically does not induce liver inflammation, short-term fasting triggered hepatic inflammation and compensatory proliferation in hepatocyte-specific RIPK1-deficient (*Ripk1*$^{\Delta hep}$) mice. Transcriptomic analysis revealed that short-term fasting oriented the hepatic microenvironment into an inflammatory state in *Ripk1*$^{\Delta hep}$ mice, with upregulated expression of inflammation and immune cell recruitment-associated genes. Single-cell RNA sequencing further confirmed the altered cellular composition in the liver of *Ripk1*$^{\Delta hep}$ mice during fasting, highlighting the increased recruitment of macrophages to the liver. Mechanically, our results indicated that ER stress was involved in fasting-induced liver injury in *Ripk1*$^{\Delta hep}$ mice. Overall, our findings revealed the role of RIPK1 in maintaining liver homeostasis during metabolic fluctuations and shed light on the intricate interplay between cell death, inflammation, and metabolism.

Keywords： Fasting; RIPK1; liver homeostasis; inflammation; ER stress

Introduction

During the long evolutionary history, mammals have frequently encountered various metabolic stresses arising from fluctuations in food availability. The liver, functioning as the central hub for metabolism, exhibits remarkable adaptability in maintaining both hepatic and systemic homeostasis when faced with these metabolic challenges [1]. Acute fasting, as one of the main causes of metabolic stress, is known to trigger hepatic glycogen depletion, increased production of hepatic glucose and ketone bodies, adipose tissue lipolysis, and the influx and accumulation of lipids in the liver [2-4]. Under normal circumstances, the liver possesses the capability to shield itself from hepatic lipotoxicity caused by the elevated lipid influx and accumulation during fasting [5, 6]. However, in specific situations, such as observed in patients with anorexia nervosa, fasting can result in severe liver damage and dysfunction[7]. Nevertheless, the underlying mechanisms that dictate the liver's adaptive ability to mitigate or succumb to lipotoxicity induced by metabolic stress are not fully understood.

The serine/threonine kinase RIPK1 is a crucial mediator of cell death and inflammation [8]. It manifests two distinct, even opposing functions: its scaffold function regulates cell survival and activation of NF-κB pathway, while its kinase activity promotes cell death including apoptosis and necroptosis [9, 10]. Both functions play crucial regulatory roles across a spectrum of physiological and pathological scenarios. Notably, the kinase activity of RIPK1 has been extensively studied due to its association with the deleterious effects in pathological situations [11-14]. In contrast, the scaffold function of RIPK1 is less studied and current evidences suggest that it plays an essential role in maintaining tissue homeostasis within physiological context [15, 16]. The scaffold function of RIPK1 has been studied using *Ripk1*$^{-/-}$ cells or RIPK1 deficient mice [15-19]. The postnatality death of *Ripk1*$^{-/-}$ mice suggested that the scaffold function of RIPK1 plays an essential role in normal development, acting as a brake to prevent cell death and inflammation in different tissues [17-19]. Deletion of RIPK1 results in the loss of its scaffold function and unleashes the release of subsequent deleterious part with cell death and inflammation. Generation of conditional knockout mice with RIPK1 deletion in different tissues or cell types results in different phenotypes, suggesting that the role of RIPK1 scaffold in different tissues is dependent on the context in tissue or cells [20-23]. In contrast to the severe phenotype observed in mice with RIPK1 deletion in epithelial cells, mice lacking RIPK1 in hepatocytes (*Ripk1*$^{\Delta hep}$) exhibit a surprising state of health and normal under steady conditions [20, 21]. Nonetheless, when confronted with pathogen-associated molecular patterns (PAMPs) or viral challenges, *Ripk1*$^{\Delta hep}$ mice display heightened inflammation and cell death [20, 24, 25]. However, the precise role of hepatocellular RIPK1 in liver

physiology remains unknown.

This study aimed to investigate the physiological functions of RIPK1 in the liver. Hepatocyte-specific RIPK1-deficient mice (*Ripk1*$^{\Delta hep}$) were generated and subjected to a 12-hour fasting period. Surprisingly, we observed that RIPK1 deficiency in hepatocytes sensitized the liver to acute liver injury and hepatocyte apoptosis. Remarkably, both male and female *Ripk1*$^{\Delta hep}$ mice exhibited fasting-induced liver injury and apoptosis, emphasizing the robustness of this phenotype across genders. Furthermore, short-term fasting triggered hepatic inflammation in *Ripk1*$^{\Delta hep}$ mice, as indicated by elevated expression of inflammatory markers and increased compensatory proliferation, potentially linked to hepatocellular carcinoma markers.

Transcriptomic profiling of liver tissues revealed that RIPK1 deficiency amplified the proinflammatory response during fasting, with upregulated expression of inflammation-associated genes and enhanced recruitment of immune cells to the liver. Single-cell RNA sequencing further dissected the altered cellular composition in *Ripk1*$^{\Delta hep}$ mice, highlighting an expansion of recruited macrophages and NK&T cells. Sub-clustering of macrophages unveiled an increased presence of recruited macrophages in *Ripk1*$^{\Delta hep}$ mice during fasting, suggesting their role in driving the fasting-induced inflammatory state. In summary, our study sheds light on the critical role of RIPK1 in maintaining liver homeostasis during short-term fasting and provides insights into the intricate interplay between cell death, inflammation, and liver adaptation to metabolic challenges.

Material & Methods

2.1 Key Resources Table

REAGENT or RESOURCE	SOURCE	IDENTIFIER
Critical Commercial Assays		
Serum alanine transaminase (ALT)	Nanjing Jiancheng Bioengineering Institute	C009-2-1
Serum aspartate transaminase (AST)	Nanjing Jiancheng Bioengineering Institute	C010-2-1
Serum triglyceride (TG)	Nanjing Jiancheng Bioengineering Institute	A110-1-1
Serum cholesterol (TC)	Nanjing Jiancheng Bioengineering Institute	A111-1-1
Serum free fatty acid (FFA)	Solarbio	BC0595
Ketone Body Assay Kit	Abcam	ab272541
Hepatic triglyceride (TG)	Solarbio	BC0625
TUNEL Assay Kits	Vazyme	A113-02
Antibodies		

anti-cleaved-Caspase-3	Cell Signaling Technology	9661S
anti-phospho-MLKL (S345)	Cell Signaling Technology	37333S
anti-F4/80	Servicebio	GB113373
anti-CD11b	Servicebio	GB11058
anti-CCR2	Servicebio	GB11326
anti-CX3CR1	Servicebio	GB11861
anti-Ki67	Bioss	bs-2130R
anti-Alb	Servicebio	GB122080
anti-TNFα	proteintech	60291-1-Ig
anti-RIPK1	Cell Signaling Technology	3493S
anti-phospho-IRE1α	Abcam	ab48187
anti-IRE1α	Cell Signaling Technology	3294S
anti-GRP78	Cell Signaling Technology	3177S
anti-CHOP	Cell Signaling Technology	2895S
anti-GAPDH	Servicebio	GB12002

2.2 Mouse models

Ripk1$^{fl/fl}$ and *Albumin-cre* transgenic mice on C57BL/6J background as previously described were kindly provided by Prof. Haibing Zhang (Chinese Academy of Sciences, Shanghai, China), both male and female littermates were used in the experiments [26]. Liver-specific RIPK1 knockout mice (*Ripk1*$^{\Delta hep}$ mice) were generated by crossing *Ripk1*$^{fl/fl}$ and *Albumin-cre* mice. Then *Ripk1*$^{fl/fl}$ mice were bred with *Ripk1*$^{fl/fl\ Cre/+}$ mice to generate *Ripk1*$^{fl/fl}$ and *Ripk1*$^{fl/fl\ Cre/+}$ mice as littermates. All mice were maintained in the standard laboratory conditions with temperature 22±2℃, strict 12 hours dark-light cycles (7:00 a.m. to 7:00 p.m.). All mice had ad libitum access to food and water, and before the start of experiments all mice were maintained on a regular chow diet (LAD 0011, Trophic Animal Feed, China). All experiments were conducted following the Animal Care and Use Committee at Nanjing University of Science & Technology.

For the fasting studies involving *Ripk1*$^{fl/fl}$ and *Ripk1*$^{\Delta hep}$ mice, 6-week-old littermates of *Ripk1*$^{fl/fl}$ or *Ripk1*$^{\Delta hep}$ were randomly assigned to groups. The fed group was allowed ad libitum access to both food and water. The fasted group, on the other hand, was deprived of food but not water from 8:00 p.m. since then, and this deprivation continued for a period of 12 hours.

For the endoplasmic reticulum stress inhibitor experiment, 6-week-old *Ripk1*$^{fl/fl}$ and *Ripk1*$^{\Delta hep}$ mice were divided into separate groups and administered either 80 mg/kg of 4-PBA (SML0309, Sigma, Germany) or saline vehicle via intraperitoneal injection at 8:00 a.m. Fasting was initiated for all groups by removing food at 8:00 p.m., while water was still available, for a duration of 12 hours. At 10:00 p.m., the mice were

intraperitoneally injected with 80 mg/kg of 4-PBA.

For the high-fat diet (HFD) experiment, separate groups of *Ripk1*$^{fl/fl}$ and *Ripk1*$^{\Delta hep}$ mice were fed either a HFD (TP201482; Trophic Animal Feed, China) or a normal diet (LAD 0011, Trophic Animal Feed, China) for a period of 6 days. On the last day, a 3-hour fast was initiated at 7 a.m. and the mice were sacrificed thereafter.

For the adenovirus-associated virus (AAV) experiment, 6-week-old littermates of *Ripk1*$^{fl/fl}$ were randomly divided into two groups. One group was administered serotype 8 AAV-thyroxine-binding globulin (TBG)-Cre (AAV-TBG-Cre, 1.5×10^{11} gene copies per mouse, intravenously) (H5721, Obio Technology, China), while the other group was injected with AAV-TBG-null (H20594, Obio Technology, China). After 4 weeks, the mice were subjected to the same fasting rationale as described earlier.

At the end of the experiment of each different model, mice were sacrificed following blood collection. Subsequently, the mice were dissected and the liver tissues were harvested. Some portions of the tissues were fixed in 4% paraformaldehyde tissue fixation solution for further histological examination, while others were stored at -80 °C for additional detection. All mice used for experiments displayed general health. The total number of mice analyzed for each experiment is detailed in the figure legends.

2.3 Serum and liver assays

Plasma was maintained at room temperature for 1 h, and then centrifuged at 4,000 rpm for 10 min to take the supernatant as serum. Serum alanine transaminase (ALT), aspartate transaminase (AST), triglyceride (TG), cholesterol (TC), free fatty acid (FFA) and β-hydroxybutyrate (BOH) were measured according to the manufacturer's instructions. For measurements of liver triglyceride (TG) levels, 50 mg liver was homogenized in lysis buffer (isopropanol: chloroform = 1:1) using a high speed low temperature tissue grinding machine (Servicebio, China) and supernatant was centrifuged 8,000 g for 10 min at 4℃ for measurement according to the manufacturer's instructions.

2.4 TUNEL assay

TUNEL Assay Kits were used to measure apoptotic cells in livers. Briefly, paraffin-embedded liver tissue sections were dried for 30 min at 60 °C, and soaked in xylene to deparaffinized completely. Deparaffinized sections were pretreated by proteinase K for 20 min at 25 °C. Then PBS was used to wash tissue sections and the mixture of reaction buffer with TdT enzyme was used to incubate in dark for 60 min at 25 °C. Meanwhile the cell nucleuses were stained with DAPI. The tissue sections were observed and photographed using the fluorescence microscope (NIKON ECLIPSE 80i). The number of apoptotic cells was quantified in at least three random fields of the same size.

2.5 RNA isolation and RT-qPCR

Liver tissue (10-20 mg) was homogenized directly in TRIzol (Invitrogen) using a high speed low temperature tissue grinding machine (Servicebio, China), then total mRNA was extracted according to the manufacturer's instructions. Next cDNA was synthesized using one-step reverse transcription kit (5x All-In-One-RT Naster Mix, Abm). RT-qPCR reactions were performed on the iQ5 real-time PCR system (Bio-Rad, USA) using Hieff™ qPCR SYBR® Green Master Mix (Yeasen Biotech, China). GAPDH mRNA was used as an internal control to normalize mRNA expression. The sequences of primers for qPCR were as follows:

Name	Forward (5′-3′)	Reverse (5′-3′)
Mcp-1	CACTCACCTGCTGCTACTCA	AGACCTTAGGGCAGATGCAG
Tnfα	GTAGCCCACGTCGTAGCAAA	TAGCAAATCGGCTGACGGTG
Il-1β	GCCACCTTTTGACAGTGATGAG	ACGGGAAAGACACAGGTAGC
Ifnγ	ATGAACGCTACACACTGCATC	CCATCCTTTTGCCAGTTCCTC
Il-6	TGATGGATGCTACCAAACTGGA	GGAAATTGGGGTAGGAAGGACT
Afp	ACCTCCAGGCAACAACCATT	GTTTGACGCCATTCTCTGCG
Ki67	AACCATCATTGACCGCTCCT	AGGCCCTTGGCATACACAAA
Grp78	CGAGGAGGAGGACAAGAAGG	TCAAGAACGGGCAAGTTCCAC
Xbp1s	GAGTCCGCAGCAGGTG	AGGGTACCTGAGACTGTG
Chop	CTGCCTTTCACCTTGGAGAC	ATAGAGTAGGGGTCCTTTGC
Gapdh	AGGTCGGTGTGAACGGATTTG	TGTAGACCATGTAGTTGAGGTCA

2.6 Histological analysis

Liver tissues were fixed in 4% paraformaldehyde and embedded in paraffin for immunohistochemistry/immunofluorescence. For histopathology, frozen sections of liver tissues were stained by Oil Red O working solution to determine the steatosis in liver tissues.

2.7 Immunohistochemistry and immunofluorescence analysis

For immunohistochemistry in liver tissues, paraffin embedded mouse liver sections (3.5 - 4 μm) were dried for 30 min at 60 °C, and soaked in xylene to deparaffinized completely. Then boiled the liver sections in citrate buffer (pH = 6.0) for antigen retrieval, followed by hydrogen peroxide blocking of endogenous

peroxidase. Then sections were incubated with primary antibody (anti-Ki67) at 4 °C overnight. The slides were then washed with PBS (PH=7.4) and incubated with secondary antibody for 1 h at 25°C, and then stained with DAB substrate after 5 min with streptavidin-HRP. The cell nuclei were stained with hematoxylin for 3 min at 25°C. For immunofluorescence, after being incubated with primary antibodies (anti-cleaved-Caspase-3, anti-phospho-MLKL (S345), anti-F4/80, anti-CD11b, anti-CCR2 and anti-CX3CR1) at 4 °C overnight, slides were washed with PBS (PH = 7.4) for three times and then incubated with fluorescent secondary antibodies in dark for 60 min at 25°C. The cell nuclei were stained in dark by DAPI for 5 min at 25°C. Finally, the slides were observed and photographed using the fluorescence microscope (NIKON ECLIPSE 80i). The number of positive cells was quantified in at least three random fields of the same size.

2.8 Western blotting

Total protein was extracted from liver tissues with RIPA lysis buffer (Beyotime, China) with protease inhibitor (P1005; Beyotime, China) and phosphatase inhibitor (P1081; Beyotime, China). BCA Protein Assays kits(Yeasen, China) were used to measure the protein concentrations. Equal amounts of proteins were separated on sodium dodecyl sulfate–polyacrylamide gel electrophoresis (SDS-PAGE) on 4–12% acrylamide gel (Yeasen, China) and transferred onto 0.22 μm PVDF membranes (Millipore Corporation, USA). Membranes were incubated with primary antibodies (anti-RIP1, anti-TNFα, anti- phospho-IRE1α, anti-IRE1α, anti- GRP78 and anti-CHOP) overnight at 4°C, washed with TBS-T (0.1% TWEEN-20) and incubated with suitable secondary antibodies (Goat anti-Mouse IgG HRP or Goat anti-Rabbit IgG HRP) at room temperature for 1 h. A chemiluminescent reagent (Beyotime, China) and a ChemiDoc MP Imaging System (CLiNX, China) were used for detection.

2.9 Liver tissue transcriptome sequencing

2.9.1 Isolation of RNA for sequencing

6-week-old *Ripk1*$^{fl/fl}$ and *Ripk1*$^{\Delta hep}$ male mice were fasted for 6 weeks. At end of the fast, mice were sacrificed and dissected. Approximately 200 mg of liver tissue at the left lateral lobe was cut, weighed and harvested for each mouse. Total RNA was extracted from mouse liver using TRIzol reagent (Invitorgen) following the manufacturer's instructions. The isolated RNA was further quantified using a NanoDrop 2000 spectrophometer (ThermoFisher Scientific). Then the total RNA was subjected to sequencing for transcriptome analysis.

2.9.2 cDNA Library construction and sequencing

The RNA-seq library was generated using the TruSeq Stranded Total RNA Sample Preparation kit from Illumina (NEB, USA) following the manufacturer's recommendations for 150-bp paired-end sequencing.

Poly-A-containing mRNA were purified and fragmented from DNase-treated total RNA using oligo(dT) magnetic beads. Following the purification step, mRNAs were fragmented to 300 bp nucleotides and used for synthesis of single-stranded cDNAs by means of random hexamer priming. With the constructed single-stranded cDNAs as templates, second strand cDNA synthesis was performed to prepare double-stranded cDNAs. These cDNAs were then amplified with end-pair repair, addition of A-tail, and adapter ligation using polymerase chain reaction (PCR). The quality control of cDNA library was evaluated by Agilent 2100 BioAnalyzer (Agilent Technologies). After quality control, sequencing was performed with Illumina HiSeq3000.

2.9.3 Transcript data analysis

Illumina sequencing analysis viewer was used for data quality check and Illumina Bcl2fastq2 program was used for demultiplexing. Then the high-quality filtered sequencing data was aligned with mouse reference genome (GRCm38) by TopHat (version 2.1.1). To profile differential gene expression (DEG), reads per kilo-base per million mapped reads (RKM) were calculated for each transcript. Paired sample t-tests followed by Benjamini-Hochberg correction were performed to identify DEGs. Genes with >2-fold changes (|log2 fold change| >1) and false discovery rate <0.05 were defined as DEGs by DESeq2 (version 1.18.1). Enrichment analysis of DEGs was performed by Kyoto Encyclopedia of Genes and Genomes (KEGG) (http://www.kegg.jp/) pathway enrichment analysis to identify the affected metabolic pathways and signal transduction pathways.

2.10 Single-cell RNA sequencing

Male mice of 6 weeks old with *Ripk1*$^{fl/fl}$ and *Ripk1*$^{\Delta hep}$ genotypes were subjected to a 12-hour fast, after which they were sacrificed and dissected. Liver tissue samples were collected from the left lateral lobe, right lateral lobe, and right medial lobe of each mouse and weighed, with approximately 600 mg of tissue per sample. Liver tissue samples were mechanically dissociated and digested in lysis buffer containing collagenase/dispase and 0.001% deoxyribonuclease I, after which the samples were processed. Isolated cells passed through 70 μm cell strainer were treated with Red Blood Cell Lysis Solution (10×) (Miltenyi Biotec) for 5 min to lyse blood cells. To acquire cells with >90% viability, dead cells were removed with Dead Cell Removal Kit (Miltenyi Biotec) according to the manufacturer's instructions and cell pellet was resuspended in 2% FBS/phosphate-buffered saline. Then live cells were counted with Countstar and adjusted the cell concentration to 1000 cells/μl. For scRNA-seq, chromium microfluidic chips were loaded with cell suspension with 3′ chemistry and barcoded with a 10× Chromium Controller (10× Genomics). RNA was reverse-transcribed from the barcoded cells. Qubit dsDNA HS Assay Kit (Invitrogen) was used to quantify cDNA

concentration and single- cell transcriptome libraries were constructed using the 10× Chromium Single Cell 3′ Library (10×Genomics, v3 barcoding chemistry). Quality control was performed with Agilent 2100(Agilent Technologies). Libraries were then purified, pooled, and analyzed on Illumina NovaSeq 6000 S2 Sequencing System with 150 bp paired-end reads according to the manufacturer's instructions.

For analysis of scRNA-seq data, briefly, cellRanger single- cell software suite (v3.1.0) were used to process and analysis scRNA-seq reads with the default parameters. Base calling files generated by Illumina sequencer were demultiplexed according to the sample index. Sequences were then aligned to mouse reference genome mm10 reference for whole transcriptome analysis. CellRanger 3.1.0 were used to conducted Filtering, barcode counting, and UMI counting. For the following analysis multiple samples were aggregated. Visualization, quality control, normalization, scaling, PCA dimension reduction, clustering, and differential expression analysis were used by Loupe browser and Seurat (v4.0.0) to perform. Cells with a detected gene number of <200 or >10000, mitochondrion gene percentage of <10, hemoglobin gene percentage of <10, and doublet nucleus were removed by package Seurat (v4.0.0). Data were subsequently log-normalized (divided by the total expression and amplified scaling factor 10,000) before further analyses. The remaining 22,274 cells were unsupervised clustered after aligning the top 30 dimensions and setting resolution to 0.9. Loupe browser software (10X Genomics) were used to demonstrate UMAP and T-SNE. The identity for each cluster was assigned according to marker genes for known cell types in the mouse liver. Differentially expressed genes with absolute log-fold change greater than 1.5 and p value less than 0.05 were used for pathway and network enrichment analysis on the Kyoto Encyclopedia of Genes and Genomes website (KEGG) (http://www.kegg.jp/).

2.11 Statistical analysis

All the results in this study are expressed as mean ± standard error of the mean (SEM). Unpaired Student's t test or one/two-way ANOVA (for more than 2 groups) analysis were used to calculate the differences in mean values, using GraphPad Prism ® 8.2.1 software (San Diego, USA). $p < 0.05$ was considered as statistically significant.

Results

3.1. RIPK1 deficiency in hepatocytes sensitizes the liver to short-term fasting-induced liver injury and hepatocyte apoptosis

To investigate the physiological functions of RIPK1 in liver homeostasis, hepatocyte-specific RIPK1 deficient mice (*Ripk1*$^{\Delta hep}$ mice) were generated by crossing *Ripk1*$^{fl/fl}$ mice with Albumin-Cre transgenic mice.

Deletion of RIPK1 in hepatocytes was confirmed by the analysis of RIPK1 expression in the liver tissue (Fig. S1 A). Consistent with previous reports [20], *Ripk1*$^{\Delta hep}$ mice were normal and healthy. Then both *Ripk1*$^{\Delta hep}$ mice and their control littermates were subjected to short-term 12-hour fasting from 8:00 pm-8:00 am. To our surprise, short-term fasting induced a significant increase in serum transaminase (alanine amino-transferase (ALT) and aspartate amino-transferase (AST)) levels in *Ripk1*$^{\Delta hep}$ mice but not in their wild type controls, suggesting that RIPK1 deficiency sensitizes the liver to short-term fasting, inducing acute liver injury (Fig.1A and 1B). Since RIPK1 is a key player regulating cell death including caspase-8-mediated apoptosis and RIPK3-MLKL-mediated necroptosis, we next examined whether the liver injury was due to cell apoptosis or necroptosis. As Fig. 1C&D shown, the number of TUNEL-positive cells in the liver of *Ripk1*$^{\Delta hep}$ mice was significantly higher compared to the control mice. Cleaved caspase-3 and phospho-MLKL are widely recognized as key proteins involved in the execution of apoptosis and necroptosis, respectively, and are commonly used as markers to detect these types of cell death. As indicated in Fig.1E&F, the number of cleaved caspase-3-positive cells was significantly higher in *Ripk1*$^{\Delta hep}$ mice compared to controls. However, we did not observe any change in the number of phospho-MLKL-positive cells in *Ripk1*$^{\Delta hep}$ mice (Fig. 1G). These results suggest that fasting-induced acute liver injury in *Ripk1*$^{\Delta hep}$ mice might be due to apoptosis rather than necroptosis. To further investigate which cell types were undergoing apoptosis, we conducted the co-staining with TUNEL and Alb immunofluorescence, and the results demonstrated that most of TUNEL-positive cells co-localized with Alb-positive staining (Fig. 1H), suggesting that short-term fasting induced apoptosis mainly in hepatic parenchymal cells in *Ripk1*$^{\Delta hep}$ mice.

It is known that fasting induces hypoglycemia and adipose tissue lipolysis, leading to the release of free fatty acids, which are transported to liver to facilitate the production of ketone bodies through fatty acid beta oxidation. We next investigated whether RIPK1 deficiency in hepatocytes affected the metabolic parameters during fasting. As Fig. 1I-O shown, short-term fasting significantly decreased the blood glucose level, elevated the plasma levels of triglycerides (TG), total cholesterol (TC), free fatty acids (FFA) and β-hydroxybutyrate (BHB), and there was no obvious difference between wild type control and *Ripk1*$^{\Delta hep}$ mice, suggesting that RIPK1 deficiency did not affect the lipid metabolism in liver during fasting.

We next investigated whether sex difference affects fasting-induced acute liver injury in *Ripk1*$^{\Delta hep}$ mice. Female *Ripk1*$^{fl/fl}$ mice and their *Ripk1*$^{\Delta hep}$ littermates were subjected to short-term fasting. Consistent with male mice, we observed a significant increase in serum ALT/AST levels and hepatic TUNEL-positive cells in *Ripk1*$^{\Delta hep}$ female mice (Fig. S1B-D), suggesting that RIPK1 deficiency sensitizes the liver to short-term fasting-induced liver injury and hepatocyte apoptosis in both male and female mice.

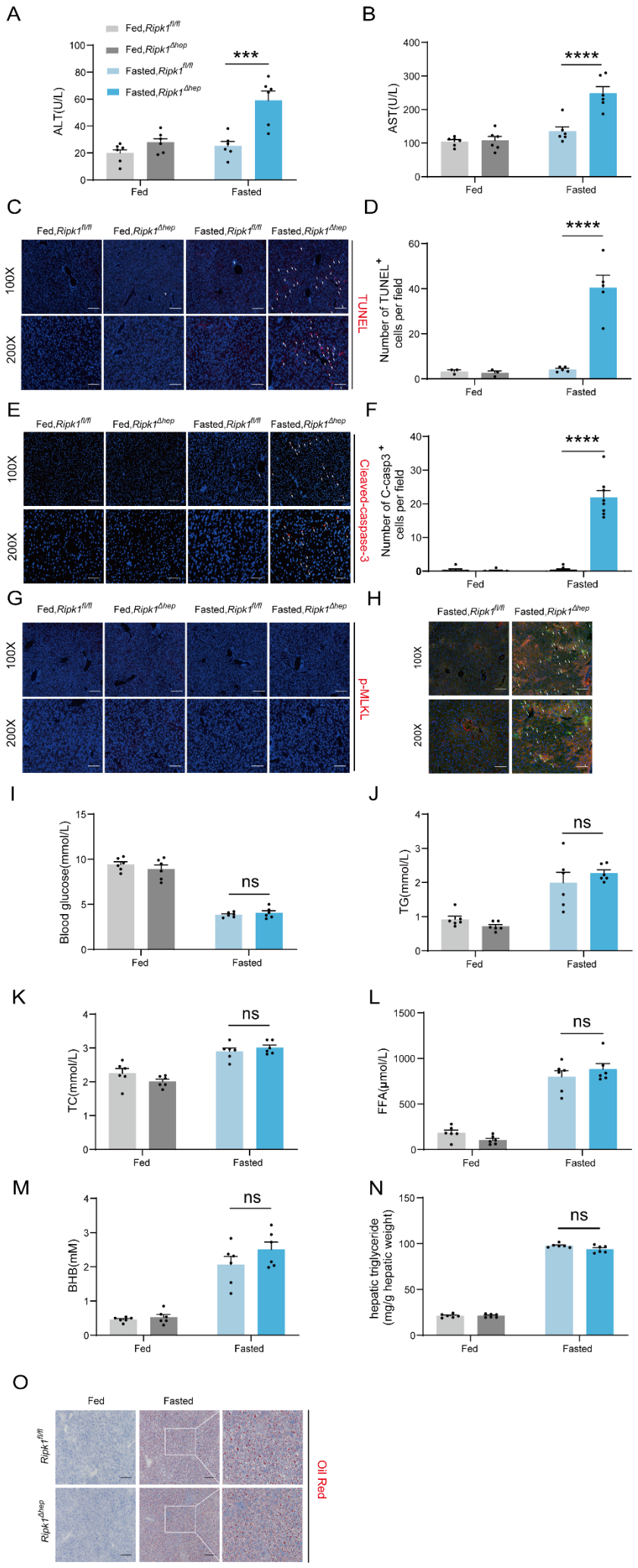
A
Fed,Ripk1fl/fl
Fed,Ripk1Δhep
Fasted,Ripk1fl/fl
Fasted,Ripk1Δhep
ALT(U/L)
***
Fed
Fasted
B
AST(U/L)
****
C
100X
200X
TUNEL
D
Number of TUNEL+ cells per field
E
Cleaved-caspase-3
F
Number of C-casp3+ cells per field
G
p-MLKL
H
I
Blood glucose(mmol/L)
ns
J
TG(mmol/L)
K
TC(mmol/L)
L
FFA(μmol/L)
M
BHB(mM)
N
hepatic triglyceride (mg/g hepatic weight)
O
Oil Red

Figure 1. RIPK1 deficiency in hepatocytes sensitizes the liver to short-term fasting-induced liver injury and hepatocyte apoptosis. (A) Serum alanine amino-transferase (ALT) levels. (B) Serum aspartate amino-transferase (AST) levels. (C&D) Representative images and quantification of TUNEL staining. Scale bar, 50 or 100 μm. (E&F) Representative images and quantification of liver sections stained with anti-cleaved caspase 3 antibody (red) and DAPI (blue). Scale bar, 50 or 100 μm. (G) Representative images of liver sections stained with anti- phospho-MLKL antibody (red) and DAPI (blue). Scale bar, 50 or 100 μm. (H) Fluorescence microscopy images of the liver stained with anti-Alb antibody (red), TUNEL (green), and DAPI (blue). Scale bar, 50 or 100 μm. (I) Blood glucose levels. (J) Serum triglycerides (TG) levels. (K) Serum total cholesterol (TC) levels. (L) Serum free fatty acids (FFA) levels. (M) Serum β-hydroxybutyrate (BHB) levels. (N) Hepatic triglyceride (TG) levels (mg/g tissue). (O) Liver tissue was stained by Oil Red O. Scale bar, 100 μm. The data was analyzed via two-way ANOVA or one-way ANOVA. Data are expressed as mean ± SEM (n=6 per group). Asterisks denote statistical significance. ns, no significant, * $P < 0.05$, *** $P < 0.001$, **** $P < 0.0001$.

3.2. Short-term fasting induced hepatic inflammation and compensatory proliferation in *Ripk1$^{\Delta hep}$* mice

As a central hub for metabolism and many other physiological processes, liver coordinates a series of adaptations to maintain tissue homeostasis during food and energy fluctuations. Normally, short-term or temporary fasting will not disrupt liver homeostasis and cause tissue cell death and inflammation. However, consistent with liver injury and hepatocyte death, short-term fasting induced hepatic inflammation in *Ripk1$^{\Delta hep}$* mice. As demonstrated in Fig. 2A, the transcriptional expression of inflammatory markers, including MCP-1, TNF-α, IFN-γ, and IL-6, was all significantly induced in *Ripk1$^{\Delta hep}$* mouse liver tissue, in contrast to wild type littermates. We also examined the protein level of TNFα by histological staining (Fig. 2B&C). As liver damage is known to activate compensatory proliferation, which is thought to promote hepatocarcinogenesis [27, 28], we also evaluated the expression of AFP, a marker gene of hepatocellular carcinoma, and Ki67, a proliferation-related antigen, and found a significant increase in both markers in *Ripk1$^{\Delta hep}$* mice after fasting (Fig. 2D). To validate these findings at the protein level, we used immunohistochemistry of Ki67 to measure the rate of compensatory proliferation in livers and found a significant increase in the number of Ki67-positive cells in *Ripk1$^{\Delta hep}$* mice after 12 hours of fasting when liver injury was detected (Fig. 2E). Taken together, these results suggested that short-term fasting ignited inflammation and caused compensatory proliferation in *Ripk1$^{\Delta hep}$* mice.

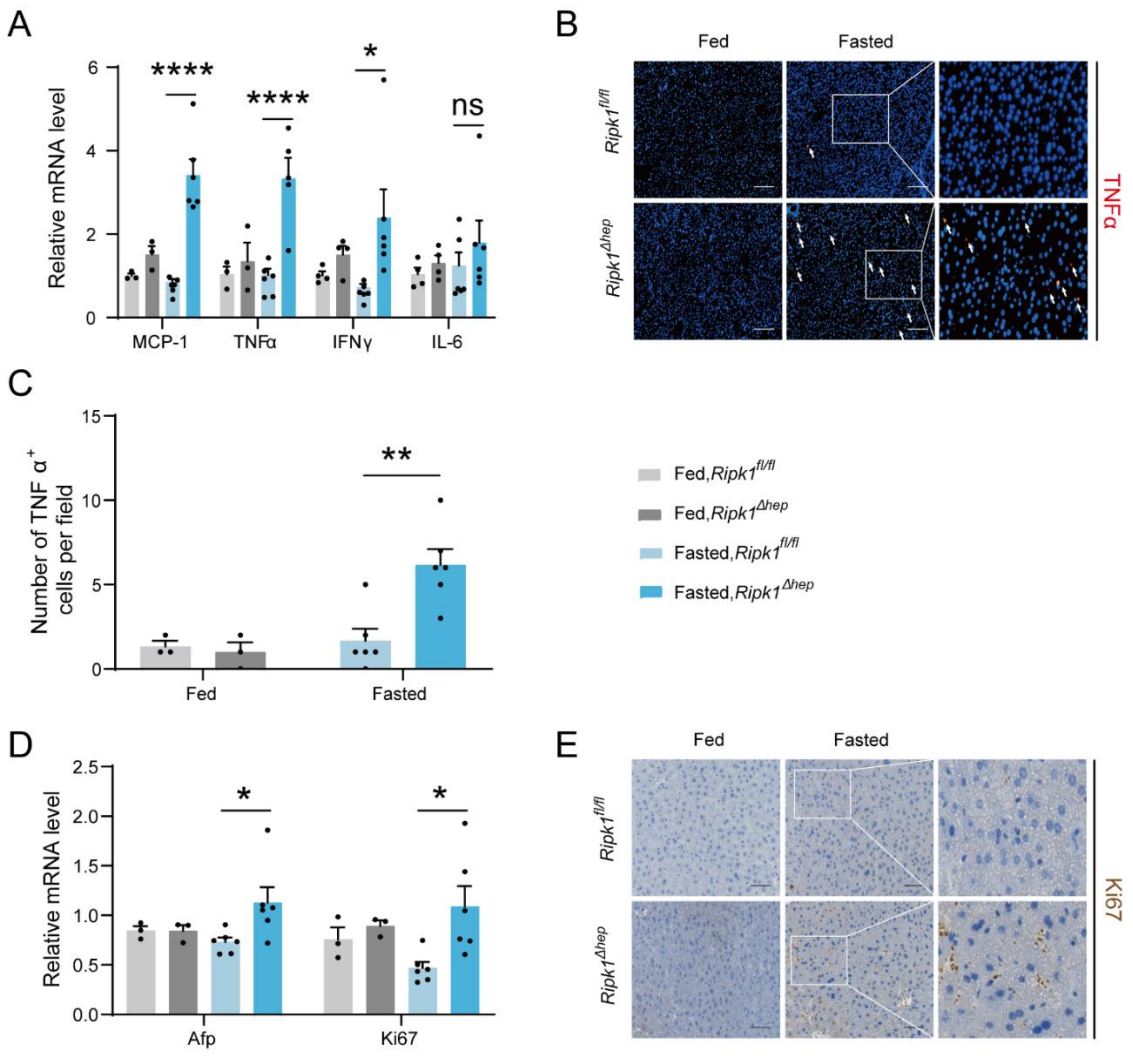

Figure 2. Short-term fasting induced hepatic inflammation and compensatory proliferation in *Ripk1*$^{\Delta hep}$ mice. (A) Hepatic mRNA expression of the inflammatory molecules. (B&C) Representative images and quantification of the liver stained with anti-TNFα antibody (red) and DAPI (blue). Scale bar, 100 μm. (D) Transcriptional expression of Afp and Ki67 in liver tissue. (E) Representative images of the liver stained with anti-Ki67 antibody (brown) and hematoxylin (blue). Scale bar, 100 μm. The data was analyzed via two-way ANOVA or one-way ANOVA. Data are expressed as mean ± SEM (n=6 per group). ns, no significant, * $P < 0.05$, *** $P < 0.001$, **** $P < 0.0001$.

3.3 Transcriptomic profile of the mouse liver tissue upon short-term fasting

We next analyzed the liver transcriptome profiles to further characterize how short-term fasting oriented the hepatic microenvironment into an inflammatory state in *Ripk1*$^{\Delta hep}$ mice. Consistent with previous reports, fasting significantly remodeled the transcriptional expression of various genes associated with metabolism in wild type mice, among which 454 genes were up-regulated and 545 genes were down-regulated (Fig. S2A). As expected, pathway enrichment (KEGG) analysis revealed that these differentially expressed genes were primarily enriched in metabolism-associated pathways, including fatty acid degradation, PPAR signaling

pathway and MAPK signaling pathway (Fig. S2B). Cluster analysis showed that fasting significantly altered metabolism-related genes in *Ripk1*$^{fl/fl}$ mice (Fig. S2C). To be noteworthy, in wild type mice, fasting normally suppressed the expression of immune- or inflammation-related genes, in agreement with the shifted energy to guarantee the need for basic survival other than immune protection during food deprivation. RIPK1 deficiency in hepatocytes did not greatly affect the gene expression profiles when food was available and there were 25 up-regulated and 54 down-regulated genes which were mostly associated with alcoholic liver disease, vascular smooth muscle contraction and cardiomyopathy in *Ripk1*$^{\Delta hep}$ mice compared to wild type control at fed state (Fig. S2D&E). However, when subjected to metabolic fluctuation with short-term fasting, loss of RIPK1 in hepatocytes amplified the affect, and there were additional 85 up-regulated and 29 down-regulated genes identified in *Ripk1*$^{\Delta hep}$ mice compared to the *Ripk1*$^{fl/fl}$ group ($p < 0.05$, $|\log2(\text{fold change})| \geq 1$) (Fig. 3A). Pathway enrichment (KEGG) analysis revealed that these differentially expressed genes (DEGs) were primarily enriched in inflammation-associated pathways, including TNF signaling pathway, IL-17 signaling pathway, toll-like receptor signaling pathway and NF-κB signaling pathway, etc. (Fig. 3B). Cluster analysis of the differentially expressed genes revealed that hepatocyte-specific deletion of RIPK1 significantly induced the expression of many genes involved in the inflammatory process after fasting, including Ccl2, Clec4e, Ikbke, and Tnfaip3 etc (Fig. 3C). Through further analysis of the transcriptome data, we observed a significant increase in the expression chemokine-related genes involved in the recruitment of immune cells, such as ITGAM, CCR2, and CX3CR1 (Fig. 3C). To validate these findings at the protein level, we conducted immunofluorescence staining for F4/80, a marker for liver-resident immune cells, and CD11b, CCR2, and CX3CR1, markers for liver-recruited immune cells. Our results demonstrated a significant increase in the number of CD11b, CCR2, and CX3CR1 positive cells in *Ripk1*$^{\Delta hep}$ mice after fasting, while F4/80 expression remained unchanged (Fig. 3D and 3E). These results suggested that in contrast to the immunosuppression state of liver during fasting, RIPK1 deficiency sensitize the liver into a proinflammatory state, with induced expression of inflammation and immune cell recruitment-associated genes. Hepatic gene expression profile reflected the dynamics of recruited macrophages into liver in *Ripk1*$^{\Delta hep}$ mice. RIPK1 might be act as an important protein to maintain the immune tolerant homeostasis in liver during metabolism changes.

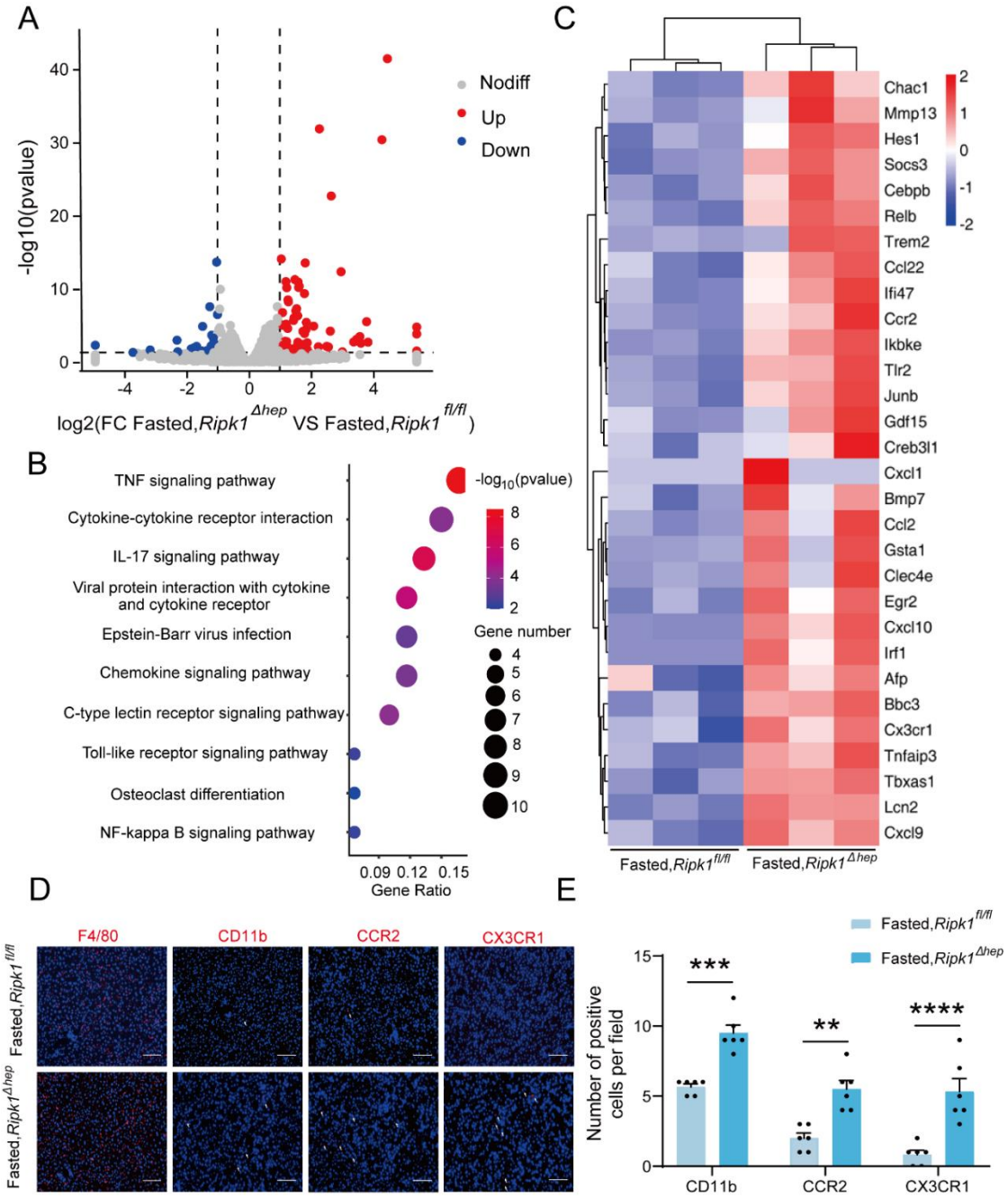

Figure 3. Transcriptome sequencing of the liver tissue from *Ripk1*$^{fl/fl}$ and *Ripk1*$^{\Delta hep}$ mice. (A) The volcano plot of differentially expressed genes was illustrated. The blue spots represent the down-regulated genes in *Ripk1*$^{\Delta hep}$ group compared with control (*Ripk1*$^{fl/fl}$) group, and the red spots represent the up-regulated genes in *Ripk1*$^{\Delta hep}$ group. (B) The altered signaling pathways were enriched by KEGG analysis. (C) The genes which expression were significantly altered in *Ripk1*$^{\Delta hep}$ group were depicted in the heat map. (D&E) Representative fluorescence microscopy images and quantification of the liver stained with anti-F4/80 antibody (red), anti-CD11b antibody (red), anti-CCR2 antibody (red), anti-CX3CR1 antibody (red) and DAPI (blue), respectively. Scale bar, 100 μm. The data was analyzed via two-way ANOVA or one-way ANOVA. Data are expressed as mean ± SEM (n=6 per group). ns, no significant, * $P < 0.05$, *** $P < 0.001$, **** $P < 0.0001$.

3.4. Single-cell RNA sequencing analysis of the mouse liver tissue

Transcriptomic profiling of whole liver tissue revealed that hepatic inflammation induced by fasting in *Ripk1*$^{\Delta hep}$ mice was likely arising from enhanced recruitment of immune cells to the liver. To confirm this hypothesis, we performed single-cell RNA sequencing of liver non-parenchymal cells isolated from *Ripk1*$^{\Delta hep}$ or *Ripk1*$^{fl/fl}$ mice upon fasting. A total of 22274 single-cell transcriptomes (10374 *Ripk1*$^{fl/fl}$; 11900 *Ripk1*$^{\Delta hep}$) were obtained, and thirty major clusters were identified by T-distributed stochastic neighbor embedding (t-SNE) visualization, representing different cell types based on marker gene expression (Fig. 4A &B). As the result shown, short-term fasting led to significant changes in the cellular composition of the liver in *Ripk1*$^{\Delta hep}$ mice, characterized by an increase in the number of cells in clusters 12, 14, 19, 22, and 28 and a decrease in the number of cells in clusters 9, 11, 22, 26, and 29, compared to control mice (Fig. 4C &4D). In order to further explore the significance of these changes, we identified 8 major cellular clusters in 12-hour fasted control liver, including B cells (Cd19, Cd79a, Fcmr, Cd79b, Ebf1), neutrophils (S100a8, Csf3r, S100a9, Mmp9), ECs (Igfbp7, Ptprb, Clec4g, Kdr), PCs(SDC1, CD138), DCs (Ly6d, Siglech, Rnase6, H2-Ab1), NK&T cells (Nkg7, Xcl1, Cd3d, Gzma), macrophages (Adgre1, Csf1r, Sdc3, Ifitm2) and hepatocytes (Alb, Saa1, Apoc1, Mup20) (Fig. 4E) [29, 30]. As the result shown, the numbers of macrophages and NK&T cells were increased in the liver of *Ripk1*$^{\Delta hep}$ mice compared to that of *Ripk1*$^{fl/fl}$ mice upon short-term fasting, suggesting the dynamics of recruited immune cells into liver in *Ripk1*$^{\Delta hep}$ mice (Fig. 4F). We next focused on liver macrophages, which might contribute to the fasting-induced inflammatory state in *Ripk1*$^{\Delta hep}$ mice.

As expected, pathway enrichment (KEGG) analysis based on macrophage differential genes revealed that these differentially expressed genes were primarily enriched in inflammation-associated pathways, including IL-17 signaling pathway, Antigen processing and presentation and TNF signaling pathway, etc. (Fig. 4G). We performed sub-clustering of macrophages to further dissect changes in the landscape of macrophages upon RIP1 deficiency in hepatocytes. This cluster can be further divided into two groups of cells representing liver-resident macrophages (LrMs: KCs) and recruited macrophages (RMs) based on their marker gene expression profile (Fig. 4H). LrMs were characterized by high expression of Adgre1 (encoding F4/80) and Clec4f, whereas RMs exhibited high expression of Itgam (encoding Cd11b, an important marker gene of bone marrow derived macrophages), Ccr2 (a chemokine receptor important for infiltration of circulating monocytes) and CX3CR1[31]. We observed that while the number of LrMs remained almost unchanged in *Ripk1*$^{\Delta hep}$ mice after short-term fasting compared to *Ripk1*$^{fl/fl}$ mice, the number of RMs significantly increased (Fig. 4I). These results suggested that in *Ripk1*$^{\Delta hep}$ mice compared to wild type mice, fasting induced hepatic inflammation was characterized by altered hepatic gene expression profiles and changed liver cell compartment, with increased immune cells in liver.

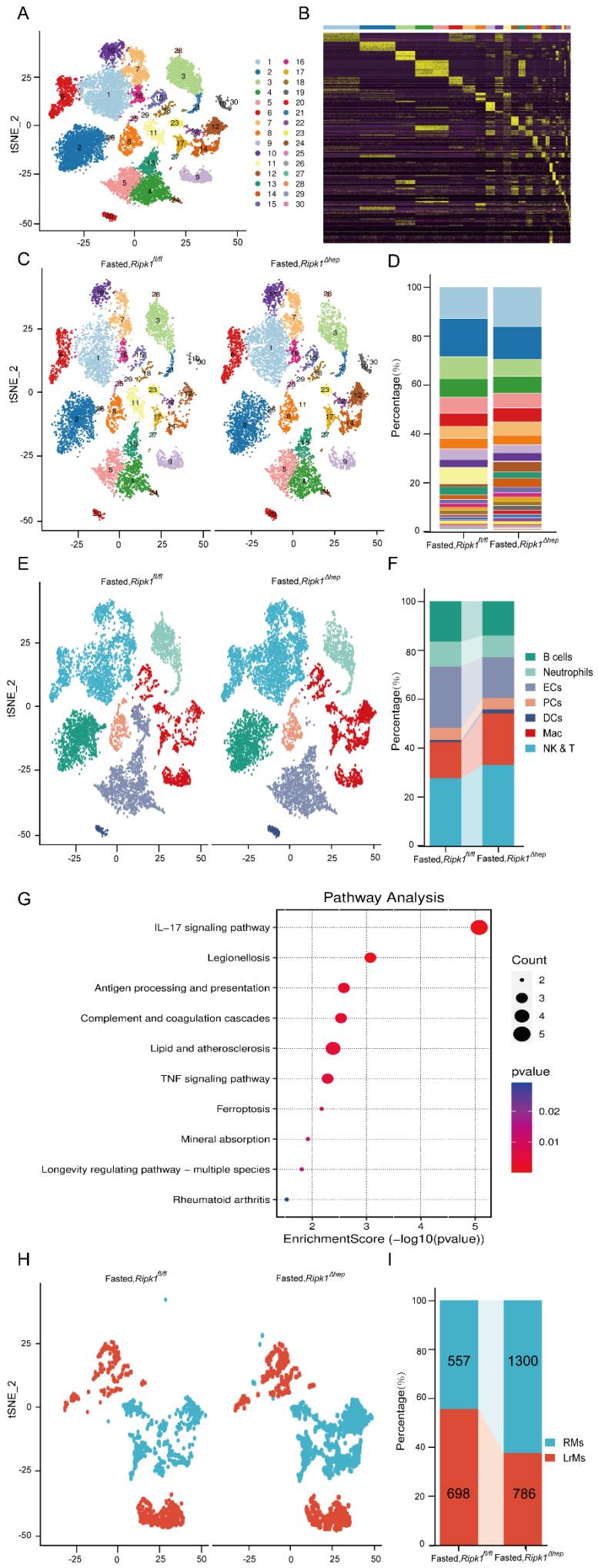
A
B
C
D
E
F
G
H
I
tSNE_2
Fasted,Ripk1fl/fl
Fasted,Ripk1Δhep
Percentage(%)
B cells
Neutrophils
ECs
PCs
DCs
Mac
NK & T
Pathway Analysis
IL−17 signaling pathway
Legionellosis
Antigen processing and presentation
Complement and coagulation cascades
Lipid and atherosclerosis
TNF signaling pathway
Ferroptosis
Mineral absorption
Longevity regulating pathway − multiple species
Rheumatoid arthritis
EnrichmentScore (−log10(pvalue))
Count
pvalue
557
1300
698
786
RMs
LrMs

Figure 4. Single-cell RNA sequencing of the liver tissue from *Ripk1*$^{fl/fl}$ and *Ripk1*$^{\Delta hep}$ mice. (A) t-SNE visualization of liver cell clusters based on 22274 single-cell transcriptomes. (B) Heatmap of cluster marker genes. (C) t-SNE plots display color-coded cell clusters of cells in the *Ripk1*$^{fl/fl}$ (left) and *Ripk1*$^{\Delta hep}$ (right) mice liver tissues. (D) Bar charts show the proportion of major cell clusters among all cells at different genotypes after fasting by scRNA-seq. (E) t-SNE plots display color-coded cell subtypes of cells in the *Ripk1*$^{fl/fl}$ (left) and *Ripk1*$^{\Delta hep}$ (right) mice liver tissues. (F) Bar charts display the proportion of major cell subtypes within all different genotypes after fasting. (G) The altered signaling pathways associated with differential gene changes in macrophages were enriched by KEGG analysis. (H) t-SNE plots display color-coded cell subtypes of macrophages in the *Ripk1*$^{fl/fl}$ (left) and *Ripk1*$^{\Delta hep}$ (right) mice liver tissues. (I) Bar charts display the proportion of major cell subtypes within macrophages after fasting.

3.5. Endoplasmic reticulum stress is required for fasting-induced liver injury and inflammation in *Ripk1*$^{\Delta hep}$ mice

We next aimed to investigate the underlying mechanism of short-term fasting-induced liver injury and inflammation in *Ripk1*$^{\Delta hep}$ mice. It is known that fasting-induced lipolysis in peripheral adipose tissue will lead to hepatic lipid burden, and excessive free fatty acids deposition has been shown to induce endoplasmic reticulum stress (ER stress) in liver. In addition, previous studies have shown that RIPK1 promotes apoptosis in response to unresolved ER stress [32]. As Fig. 1N&O indicated, the fasting strategy we employed indeed increased the lipid content in liver tissue. We also detected the expression of ER stress markers in the liver tissues of fed- or fasted-mice, respectively. As Fig. 5A indicated, short-term fasting indeed increased the expression of CHOP, GRP78, IRE1a and phosphor-IRE1a at protein levels, suggesting that short-term fasting caused ER stress in liver. To investigate whether ER stress is involved in the fasting-induced liver injury in *Ripk1*$^{\Delta hep}$ mice, *Ripk1*$^{fl/fl}$ and *Ripk1*$^{\Delta hep}$ mice were pretreated with the ER stress inhibitor 4-PBA and then the mice were subjected to short-term fasting for 12 hours (Fig. 5B). As Fig. 5C shown, 4-PBA treatment successfully reduced the expression of ER stress markers, confirming the efficiency of 4-PBA to inhibit ER stress. Interestingly, 4-PBA pretreatment effectively reduced serum ALT/AST levels and the number of TUNEL-positive cells in the liver of fasted *Ripk1*$^{\Delta hep}$ mice, suggesting that ER stress was involved in fasting-induced liver injury and hepatocyte apoptosis in *Ripk1*$^{\Delta hep}$ mice (Fig. 5D-5F). Furthermore, 4-PBA pretreatment also effectively inhibited the increased expression of inflammatory markers (MCP-1, TNF-α, IFN-γ and IL-6) and proliferation markers AFP in the liver tissue of fasted *Ripk1*$^{\Delta hep}$ mice (Fig. 5G&H).These results indicated that 4-PBA not only prevented hepatocyte apoptosis and liver injury induced by fasting in *Ripk1*$^{\Delta hep}$ mice, but also mitigated the hepatic inflammation and compensatory proliferation, suggesting that ER stress was involved in the process of fasting-induced liver injury and inflammation in *Ripk1*$^{\Delta hep}$ mice.

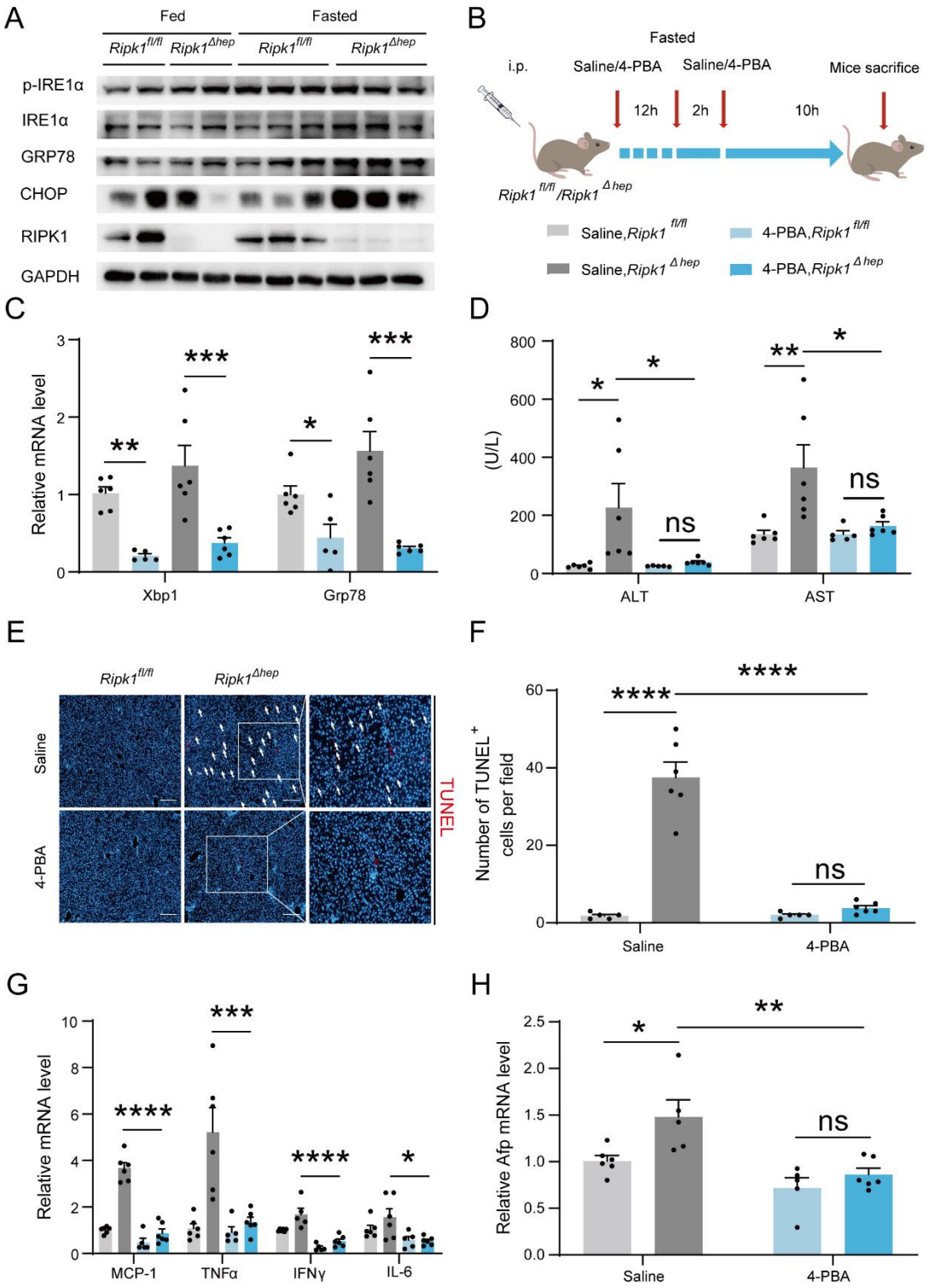

Figure 5. Inhibitor of ER stress 4-PBA effectively rescued the fasting-induced liver injury and inflammation in *Ripk1*$^{\Delta hep}$ mice. (A) Western blot analysis of p-IRE1α, IRE1α, GRP78, CHOP, RIPK1 and GAPDH in liver tissue. (B) Experiment schema. (C) Transcriptional expression of ER stress genes in mouse liver. (D) Serum alanine amino-transferase (ALT) and aspartate amino-transferase (AST) levels. (E&F) Fluorescence microscopy image and quantification of TUNEL staining. Scale bar, 100 μm. (G) Expression (qPCR) of inflammatory genes in the livers. (H) Expression (qPCR) of Afp in the livers. The data was analyzed via two-way ANOVA or one-way ANOVA. Data are expressed as mean ± SEM (n=4-6 per group). ns, no significant, * $P < 0.05$, *** $P < 0.001$, **** $P < 0.0001$.

3.6. AAV-TBG-Cre-mediated liver-specific RIPK1 knockout confirms fasting-induced acute liver injury in mice

We employed another different approach to conditionally delete RIPK1 from hepatocytes by injecting AAV8-TBG-Cre virus into *Ripk1*$^{fl/fl}$ mice. Four weeks after virus injection, the mice were subjected for short-term fasting as above studies, and then serum and liver tissue were harvested (Fig. 6A). Immunoblot analysis confirmed that RIPK1 was specifically deleted in hepatocytes by AAV8-TBG-Cre virus treatment, in contrast to the control virus AAV8-TBG-null (Fig. 6B). Our results indicated that AAV8-TBG-Cre virus-induced RIPK1 deficient mice phenocopied *Ripk1*$^{\Delta hep}$ mice, that hepatocyte-specific loss of RIPK1 sensitized the mice to short-term fasting-induced acute liver injury and hepatocyte apoptosis (Fig. 6C-F). Consistently, there was no significant alteration in serum TG, TC and liver TG levels of *Ripk1*$^{fl/fl}$ mice injected with AAV8-TBG-Cre or control AAV8-TBG-null virus (Fig. 6G-I). We also detected the expression of ER stress markers in the liver tissue of AAV8-TBG-null or AAV8-TBG-Cre mice, respectively. As Fig. 6B&J indicated, short-term fasting indeed increased the expression of CHOP, GRP78, IRE1α and phosphor- IRE1α at both mRNA and protein levels, indicating that fasting induced the occurrence of ER stress in RIPK1-deleted livers. As demonstrated in Fig. 6B&K, transcriptional expression of inflammatory markers, including MCP-1, TNF-α and IL-1β, were also significantly induced in AAV8-TBG-Cre-mouse liver tissue, in contrast to AAV8-TBG-null-mouse. Consistent with previous results, the number of cleaved caspase-3-positive cells was significantly higher in AAV8-TBG-Cre-mouse compared to controls (Fig. 6L&M). Taken together, these results suggested that hepatocyte-specific loss of RIPK1, achieved by different strategies, made the mice fragile to metabolic disturbance, and even short-term fasting would result in liver injury, hepatocyte cell death, hepatic inflammation and ER stress.

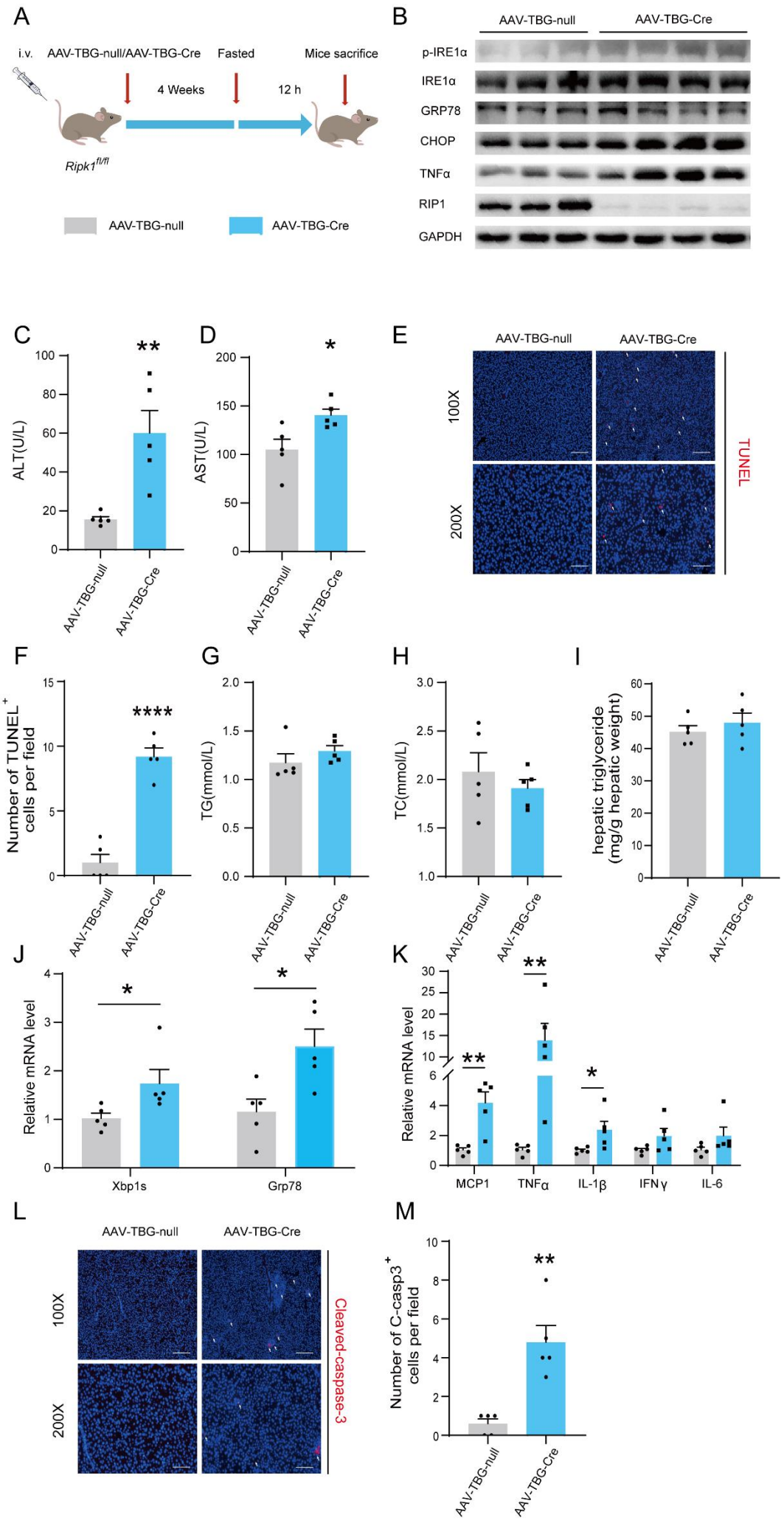
A
i.v.
AAV-TBG-null/AAV-TBG-Cre
Fasted
Mice sacrifice
4 Weeks
12 h
Ripk1fl/fl
AAV-TBG-null
AAV-TBG-Cre
B
AAV-TBG-null
AAV-TBG-Cre
p-IRE1α
IRE1α
GRP78
CHOP
TNFα
RIP1
GAPDH
C
ALT(U/L)
D
AST(U/L)
E
100X
200X
TUNEL
F
Number of TUNEL+ cells per field
G
TG(mmol/L)
H
TC(mmol/L)
I
hepatic triglyceride (mg/g hepatic weight)
J
Relative mRNA level
Xbp1s
Grp78
K
MCP1
TNFα
IL-1β
IFNγ
IL-6
L
Cleaved-caspase-3
M
Number of C-casp3+ cells per field

Figure 6. AAV-TBG-Cre-mediated liver-specific RIPK1 knockout confirms fasting-induced acute liver injury in mice (A) Schema of AAV8-TBG-Cre administration. (B) Western blot analysis of p-IRE1α, IRE1α, GRP78, CHOP, TNFα, RIPK1 and GAPDH in liver tissue. (C) Serum alanine amino-transferase (ALT) levels. (D) Serum aspartate amino-transferase (AST) levels. (E&F) Fluorescence microscopy image and quantification of TUNEL staining. Scale bar, 50 or 100 μm. (G) Serum triglycerides (TG) levels. (H) Serum total cholesterol (TC) levels. (I) Hepatic triglyceride (TG) levels (mg/g tissue). (J) Expression (qPCR) of ER stress genes in the livers. (K) Expression (qPCR) of inflammatory genes in the livers. (L&M) Fluorescence microscopy images and quantification of liver of *Ripk1*$^{\Delta hep}$ and control mice stained with anti-cleaved caspase 3 antibody (red) and DAPI (blue). Scale bar, 50 or 100 μm. The data was analyzed via two-way ANOVA or one-way ANOVA. Data are expressed as mean ± SEM (n=4-6 per group). ns, no significant, * $P < 0.05$, *** $P < 0.001$, **** $P < 0.0001$.

3.7. Short-term high fat diet feeding induced liver injury, hepatic apoptosis, inflammation and endoplasmic reticulum stress in *Ripk1*$^{\Delta hep}$ mice

We next aimed to explore whether other metabolic disturbance exhibited similar effect as short-term fasting in *Ripk1*$^{\Delta hep}$ mice. It's known that short-term fasting leads to lipolysis in adipose tissue and temporary lipid burden to hepatocytes. We therefore created a short-term high fat diet (HFD) feeding model in both wild-type control and *Ripk1*$^{\Delta hep}$ mice, to mimic the dietary-induced lipid metabolism disturbance. *Ripk1*$^{fl/fl}$ and *Ripk1*$^{\Delta hep}$ mice were fed with HFD or normal diet (ND) for 6 days respectively (Fig. 7A). We observed a significant increase in liver lipid deposition, liver triglyceride (TG), and serum total cholesterol (TC) in mice fed with HFD compared to those fed with ND (Fig. 7B-D). Previous studies reported that short-term HFD feeding was not enough to induce hepatic disorder, without obvious effects on the serum ALT/AST, liver histology, and our results with *Ripk1*$^{fl/fl}$ mice were in agreement with these findings (Fig. 7E&F). In contrast, upon 6-day HFD feeding, the serum ALT/AST levels, hepatocyte apoptosis as measured by TUNEL and hepatic inflammation were significantly elevated in *Ripk1*$^{\Delta hep}$ mice(Fig. 7E-I). Additionally, HFD feeding significantly induced the expression of AFP in *Ripk1*$^{\Delta hep}$ mice, suggesting that HFD feeding promoted tumorigenesis in *Ripk1*$^{\Delta hep}$ mice (Fig. 7J). We also found that the expression of ER stress-related genes was obviously increased in *Ripk1*$^{\Delta hep}$ mice after 6 days of HFD feeding (Fig. 7K).

Taken together, these results suggest that hepatocyte RIPK1 is essential for the maintenance of hepatic homeostasis against the disturbance induced by different metabolism behaviours, including fasting and temporary high-fat diet feeding.

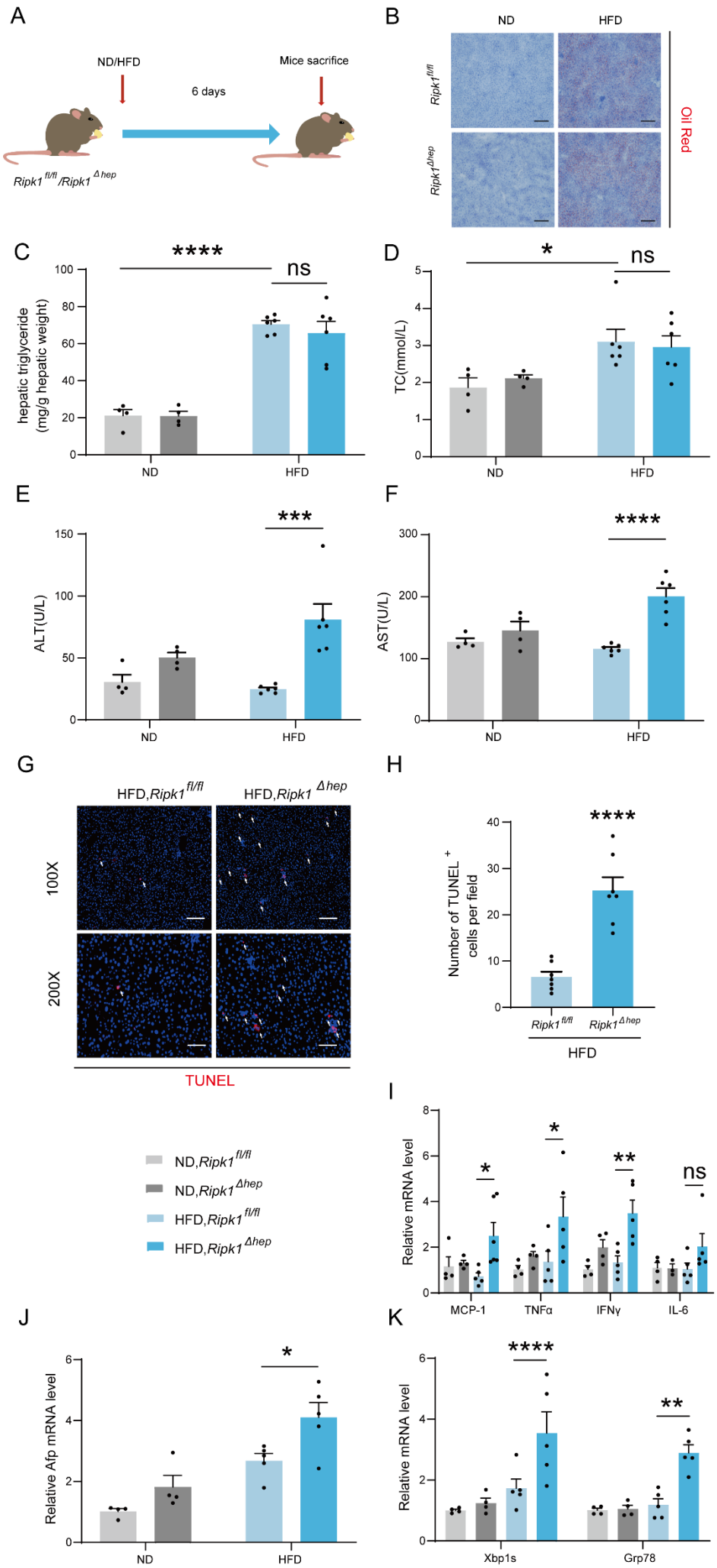
A
ND/HFD
6 days
Mice sacrifice
Ripk1 fl/fl /Ripk1 Δhep
B
ND
HFD
Ripk1 fl/fl
Ripk1 Δhep
Oil Red
C
hepatic triglyceride (mg/g hepatic weight)
****
ns
ND
HFD
D
TC(mmol/L)
*
ns
E
ALT(U/L)
***
F
AST(U/L)
****
G
HFD,Ripk1 fl/fl
HFD,Ripk1 Δhep
100X
200X
TUNEL
H
Number of TUNEL+ cells per field
****
Ripk1 fl/fl
Ripk1 Δhep
HFD
ND,Ripk1 fl/fl
ND,Ripk1 Δhep
HFD,Ripk1 fl/fl
HFD,Ripk1 Δhep
I
Relative mRNA level
MCP-1
TNFα
IFNγ
IL-6
ns
J
Relative Afp mRNA level
K
Xbp1s
Grp78

Figure 7. Short-term high fat diet feeding induced liver injury, hepatic apoptosis, inflammation and endoplasmic reticulum stress in *Ripk1*$^{\Delta hep}$ mice. (A) Schema of HFD administration. (B) Liver tissue was stained by Oil Red O. Scale bar, 100 μm. (C) Hepatic triglyceride (TG) levels (mg/g tissue). (D) Serum total cholesterol (TC) levels. (E) Serum alanine amino-transferase (ALT) levels. (F) Serum aspartate amino-transferase (AST) levels. (G&H) Fluorescence microscopy image and quantification of TUNEL staining. Scale bar, 50 or 100 μm. (I) Expression (qPCR) of inflammatory genes in the livers. (J) Expression (qPCR) of Afp in the livers. (K) Expression (qPCR) of ER stress markers in the livers. The data was analyzed via two-way ANOVA or one-way ANOVA. Data are expressed as mean ± SEM (n=4-6 per group). ns, no significant, * $P < 0.05$, *** $P < 0.001$, **** $P < 0.0001$.

4 Discussion

In this study, we demonstrated that the specific deletion of RIPK1 in hepatocytes exacerbated the liver's vulnerability to metabolic disturbances, such as short-term fasting and high-fat diet feeding, resulting in increased liver damage, apoptosis, inflammation, and compensatory proliferation. We utilized single-cell RNA sequencing and bulk RNA sequencing to characterize the hepatic cellular profiles and transcriptional profiles in response to the physiological inflammation induced by the disruption of homeostasis. Furthermore, we presented evidence indicating the involvement of ER stress in sensitizing RIPK1-deleted liver tissue. In summary, we revealed a novel physiological role of RIPK1 as a scaffold in maintaining liver homeostasis during fasting and other nutritional disturbance. These findings could prove valuable in tailoring intermittent fasting or calorie restriction regimens for specific populations based on their *Ripk1* gene polymorphism or expression profiles.

Our work shed light on the intricate interplay between cell death, inflammation, and metabolism. While the pathophysiological roles of RIPK1 have primarily been studied in inflammatory diseases and pathogen infections, emerging evidence suggests its involvement in metabolism-related pathways [15, 16, 33]. Previous studies, including our own, have linked RIPK1's kinase activity to the pathogenesis of metabolic diseases like NASH, indicating a metabolic regulatory role of RIPK1 kinase [13, 14, 34]. Subsequently, UDP-glucose 6-dehydrogenase (UGDH) and UDP-glucuronate metabolism are found to suppress NASH pathogenesis and control hepatocyte apoptosis through inhibiting RIPK1 kinase activity, further solidifying the connection between RIPK1 kinase activity and metabolism during the pathogenesis of NASH [35]. In addition to its pathological roles, RIPK1's involvement in metabolism physiology has become increasingly apparent. Mei et al. found that the postnatal lethality of *Ripk1*$^{-/-}$ mice was attributed to dysregulated aspartate metabolism, leading to impaired starvation-induced autophagy [15]. Zhang et al. recently reported that the classical energy

sensor AMPK is able to phosphorylate RIPK1 at S416 in response to metabolic stress like glucose deprivation in vitro and fasting in vivo, and this phosphorylation of RIPK1 by AMPK represents a survival mechanism to keep the kinase activity of RIPK1 in check to prevent RIPK1 kinase-mediated cell death. AMPK deficiency sensitized cells to glucose deprivation-induced cell death [33]. Their results directly linked RIPK1 to key metabolism regulator AMPK. Together with our results, it suggested that hepatic AMPK-RIPK1 axis function as a mechanism to maintain liver homeostasis during suffering metabolic stress. Moreover, *Tak1*$^{-/-}$ mice has been shown to exhibit similar phenotypes, suggesting that the key components in the complex I faction in the scaffold complex, all contribute to maintain tissue homeostasis [2]. These findings, together with our study, emphasize the critical role of RIPK1's scaffold function in sensing nutrient stress and maintaining metabolic homeostasis during various starvation conditions, both in neonatal stages and adulthood. Zhang et al. also noted that RIPK1 knockout MEFs were more susceptible to cell death induced by glucose starvation compared to WT MEFs, further underscoring the importance of RIPK1 in nutrient stress responses.

Our study also posited that hepatocyte RIPK1 plays a crucial role in preventing liver damage and inflammation triggered by metabolic stress. Prior investigations have indicated that deficiencies in TAK1 or NEMO in hepatocytes result in spontaneous liver injury and carcinogenesis in mice, with a more severe phenotype than that observed in RIPK1-deficient mice [27, 36, 37]. This is attributed to the deletion of TAK1 or NEMO unleashing the kinase activity of RIPK1, leading to the activation of RIPK1 kinase and the associated cell death pathways. Our findings, combined with these earlier studies, suggested that the RIPK1-TAK1- NF-κB axis constitutes an essential scaffold platform necessary for the liver's adaptation to metabolic fluctuations. Any improper inactivation or deletion of any component within this scaffold axis disrupts the delicate balance between cell death, inflammation, and normal function, rendering the liver vulnerable to metabolic changes and resulting in liver damage, hepatic inflammation, and compensatory proliferation.

Moreover, in contrast to organs such as the small intestine and lungs, the liver typically maintains immune tolerance and does not incite inflammation in response to various endogenous and exogenous pathogen-associated molecular patterns (PAMPs) or antigens present in the bloodstream. Recent years have witnessed the increasing attention towards physiological inflammation, which implications have been greatly broadened [38, 39]. Our research revealed that hepatocyte RIPK1 serves as a critical mechanism for preserving immune tolerance within the liver microenvironment. Furthermore, we identify an instance of physiological inflammation induced by loss of regulation in normal tissue. The physiological inflammation observed in RIPK1-deficient livers during short-term fasting is milder but akin to hepatic inflammation induced by pathogenic infections and other pathological conditions. It is characterized by the upregulation of typical

molecules, including MCP-1, TNF-α, IFN-γ, and IL-6 etc, and the recruitment of macrophages into liver tissue, indicating systemic adaptive responses.

In summary, our study revealed the multifaceted role of RIPK1 in maintaining liver homeostasis in the face of metabolic challenges, shedding light on the intricate interplay between cell death, inflammation, and metabolism. Our findings provide new insights into the role of RIPK1 in various physiological contexts.

5 Acknowledgement

This study was supported by the National Natural Science Foundation of China under Grant 22376100 and 31970897.

Reference

[1] Bernardo-Seisdedos G, Bilbao J, et al. Metabolic Landscape of the Mouse Liver by Quantitative (31) P Nuclear Magnetic Resonance Analysis of the Phosphorome [J]. Hepatology, 2021, 74(1): 148-63.

[2] Inokuchi-Shimizu S, Park E J, et al. TAK1-mediated autophagy and fatty acid oxidation prevent hepatosteatosis and tumorigenesis [J]. J Clin Invest, 2014, 124(8): 3566-78.

[3] Petersen M C, Vatner D F, et al. Regulation of hepatic glucose metabolism in health and disease [J]. Nat Rev Endocrinol, 2017, 13(10): 572-87.

[4] Zoncu R, Efeyan A, et al. mTOR: from growth signal integration to cancer, diabetes and ageing [J]. Nat Rev Mol Cell Biol, 2011, 12(1): 21-35.

[5] Fromenty B, Roden M. Mitochondrial alterations in fatty liver diseases [J]. J Hepatol, 2023, 78(2): 415-29.

[6] Cotter D G, Ercal B, et al. Impairments of hepatic gluconeogenesis and ketogenesis in PPARalpha-deficient neonatal mice [J]. Am J Physiol Endocrinol Metab, 2014, 307(2): E176-85.

[7] Rosen E, Sabel A L, et al. Liver dysfunction in patients with severe anorexia nervosa [J]. Int J Eat Disord, 2016, 49(2): 151-8.

[8] Mifflin L, Ofengeim D, et al. Receptor-interacting protein kinase 1 (RIPK1) as a therapeutic target [J]. Nat Rev Drug Discov, 2020, 19(8): 553-71.

[9] Clucas J, Meier P. Roles of RIPK1 as a stress sentinel coordinating cell survival and immunogenic cell death [J]. Nat Rev Mol Cell Biol, 2023, 24(11): 835-52.

[10] Ofengeim D, Yuan J. Regulation of RIP1 kinase signalling at the crossroads of inflammation and cell death [J]. Nat Rev Mol Cell Biol, 2013, 14(11): 727-36.

[11] Yin H, Guo X, et al. TAB2 deficiency induces dilated cardiomyopathy by promoting RIPK1-dependent apoptosis and necroptosis [J]. J Clin Invest, 2022, 132(4):

[12] Xu G, Li Y, et al. SARS-CoV-2 promotes RIPK1 activation to facilitate viral propagation [J]. Cell Res, 2021, 31(12): 1230-43.

[13] Tao L, Yi Y, et al. RIP1 kinase activity promotes steatohepatitis through mediating cell death and inflammation in macrophages [J]. Cell Death Differ, 2021, 28(4): 1418-33.

[14] Majdi A, Aoudjehane L, et al. Inhibition of receptor-interacting protein kinase 1 improves experimental non-alcoholic fatty liver disease [J]. J Hepatol, 2020, 72(4): 627-35.

[15] Mei X, Guo Y, et al. RIPK1 regulates starvation resistance by modulating aspartate catabolism [J]. Nat Commun, 2021, 12(1): 6144.

[16] Najafov A, Luu H S, et al. RIPK1 Promotes Energy Sensing by the mTORC1 Pathway [J]. Mol Cell, 2021, 81(2): 370-85 e7.

[17] Rickard J A, O'Donnell J A, et al. RIPK1 regulates RIPK3-MLKL-driven systemic inflammation and emergency hematopoiesis [J]. Cell, 2014, 157(5): 1175-88.

[18] Silke J, Rickard J A, et al. The diverse role of RIP kinases in necroptosis and inflammation [J]. Nat Immunol, 2015, 16(7): 689-97.

[19] Kelliher M A, Grimm S, et al. The death domain kinase RIP mediates the TNF-induced NF-kappaB signal [J]. Immunity, 1998, 8(3): 297-303.

[20] Filliol A, Piquet-Pellorce C, et al. RIPK1 protects from TNF-alpha-mediated liver damage during hepatitis [J]. Cell Death Dis, 2016, 7(11): e2462.

[21] Dannappel M, Vlantis K, et al. RIPK1 maintains epithelial homeostasis by inhibiting apoptosis and necroptosis [J]. Nature, 2014, 513(7516): 90-4.

[22] Imanishi T, Unno M, et al. RIPK1 blocks T cell senescence mediated by RIPK3 and caspase-8 [J]. Sci Adv, 2023, 9(4): eadd6097.

[23] Lu Y, Leng Y, et al. Endothelial RIPK1 protects artery bypass graft against arteriosclerosis by regulating SMC growth [J]. Sci Adv, 2023, 9(35): eadh8939.

[24] Filliol A, Farooq M, et al. RIPK1 protects hepatocytes from death in Fas-induced hepatitis [J]. Sci Rep, 2017, 7(1): 9205.

[25] Farooq M, Filliol A, et al. Depletion of RIPK1 in hepatocytes exacerbates liver damage in fulminant viral hepatitis [J]. Cell Death Dis, 2019, 10(1): 12.

[26] Schneider A T, Gautheron J, et al. RIPK1 Suppresses a TRAF2-Dependent Pathway to Liver Cancer [J]. Cancer Cell, 2017, 31(1): 94-109.

[27] Yang L, Inokuchi S, et al. Transforming growth factor-beta signaling in hepatocytes promotes hepatic fibrosis and carcinogenesis in mice with hepatocyte-specific deletion of TAK1 [J]. Gastroenterology, 2013, 144(5): 1042-54 e4.

[28] Inokuchi S, Aoyama T, et al. Disruption of TAK1 in hepatocytes causes hepatic injury, inflammation, fibrosis, and carcinogenesis [J]. Proc Natl Acad Sci U S A, 2010, 107(2): 844-9.

[29] Sun X, Wu J, et al. Transcriptional switch of hepatocytes initiates macrophage recruitment and T-cell suppression in endotoxemia [J]. J Hepatol, 2022, 77(2): 436-52.

[30] Zhao J, Zhang S, et al. Single-cell RNA sequencing reveals the heterogeneity of liver-resident immune cells in human [J]. Cell Discov, 2020, 6(22.

[31] Krenkel O, Tacke F. Liver macrophages in tissue homeostasis and disease [J]. Nat Rev Immunol, 2017, 17(5): 306-21.

[32] Estornes Y, Aguileta M A, et al. RIPK1 promotes death receptor-independent caspase-8-mediated apoptosis under unresolved ER stress conditions [J]. Cell Death Dis, 2014, 5(12): e1555.

[33] Zhang T, Xu D, et al. Metabolic orchestration of cell death by AMPK-mediated phosphorylation of RIPK1 [J]. Science, 2023, 380(6652): 1372-80.

[34] Yan L, Zhang T, et al. SENP1 prevents steatohepatitis by suppressing RIPK1-driven apoptosis and inflammation [J]. Nat Commun, 2022, 13(1): 7153.

[35] Zhang T, Zhang N, et al. UDP-glucuronate metabolism controls RIPK1-driven liver damage in nonalcoholic steatohepatitis [J]. Nat Commun, 2023, 14(1): 2715.

[36] Bettermann K, Vucur M, et al. TAK1 suppresses a NEMO-dependent but NF-kappaB-independent pathway to liver cancer [J]. Cancer Cell, 2010, 17(5): 481-96.

[37] Luedde T, Beraza N, et al. Deletion of NEMO/IKKgamma in liver parenchymal cells causes steatohepatitis and hepatocellular carcinoma [J]. Cancer Cell, 2007, 11(2): 119-32.

[38] Meizlish M L, Franklin R A, et al. Tissue Homeostasis and Inflammation [J]. Annu Rev Immunol, 2021, 39(557-81.

[39] Medzhitov R. The spectrum of inflammatory responses [J]. Science, 2021, 374(6571): 1070-5.

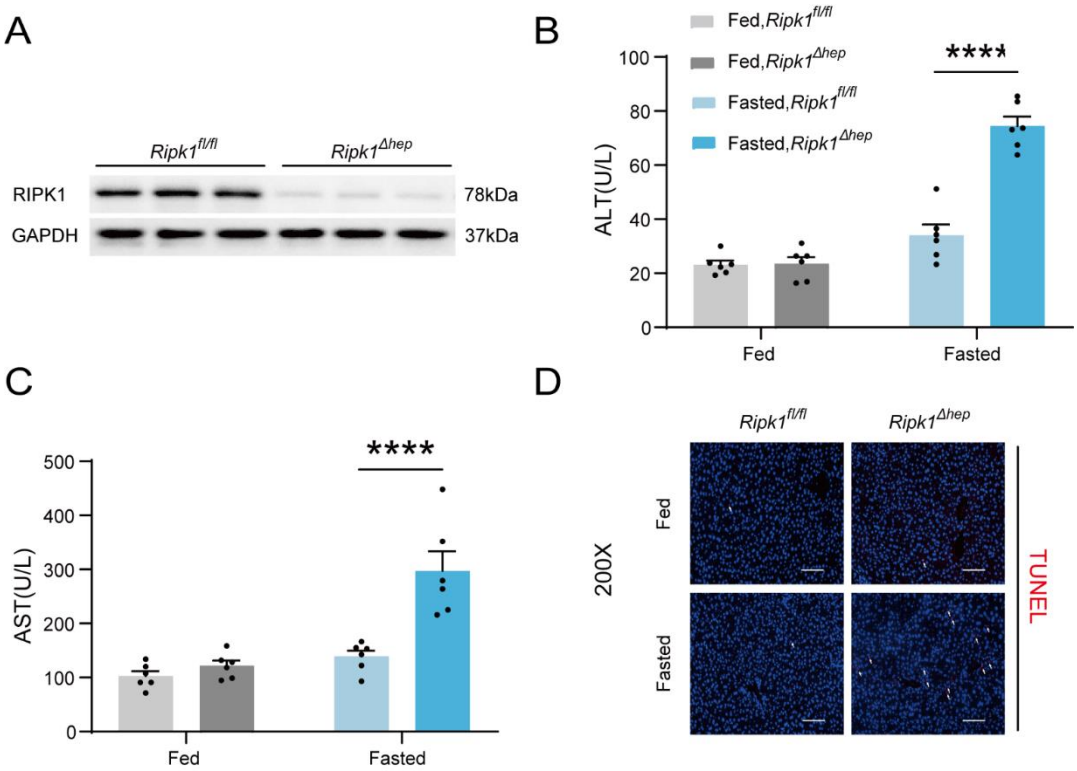

Supplementary Figure 1. RIPK1 deficiency in hepatocytes sensitizes the liver to short-term fasting-induced liver injury and hepatocyte apoptosis in female mice. (A) Western blot analysis of RIPK1 and GAPDH in liver tissue. (B) Serum alanine amino-transferase (ALT) levels. (C) Serum aspartate amino-transferase (AST) levels. (D) Representative fluorescence microscopy images of TUNEL staining. Scale bar, 50 μm. The data was analyzed via two-way ANOVA or one-way ANOVA. Data are expressed as mean ± SEM (n=4-6 per group). Asterisks denote statistical significance. ns, no significant, * $P < 0.05$, *** $P < 0.001$, **** $P < 0.0001$.

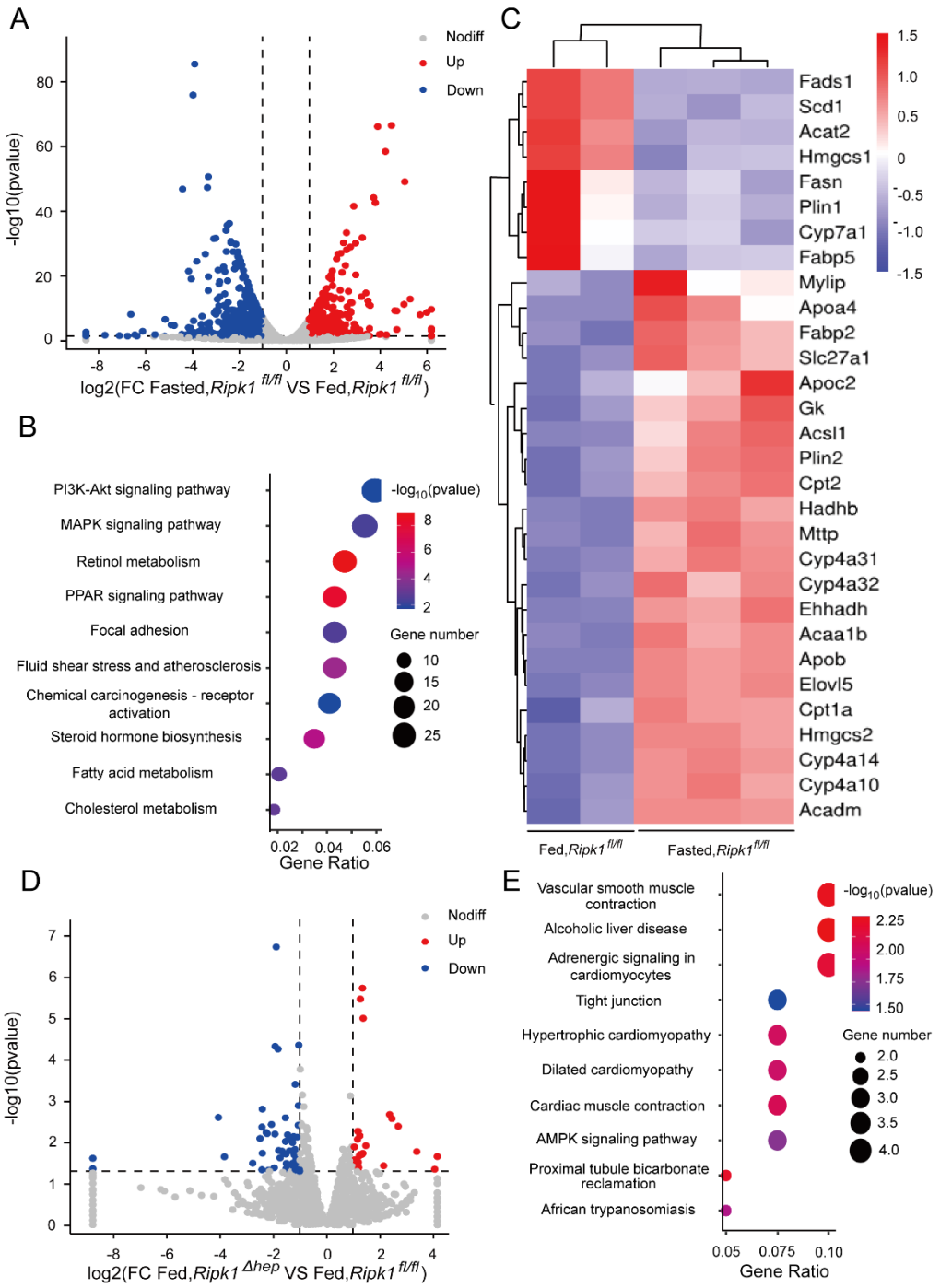

Supplementary Figure 2. Transcriptome sequencing of the liver tissue from *Ripk1*$^{fl/fl}$ and *Ripk1*$^{\Delta hep}$ mice. (A) The volcano plot of differentially expressed genes was illustrated. The blue spots represent the down-regulated genes in fasted group compared with control (fed) group and the red spots represent the up-regulated genes in *Ripk1*$^{fl/fl}$ mice. (B) The altered signaling pathways were enriched by KEGG analysis. (C) The genes which expression were significantly altered in fasted group were depicted in the heat map. (D) The volcano plot of differentially expressed genes was illustrated. The blue spots represent the down-regulated genes in *Ripk1*$^{\Delta hep}$ group compared with control (*Ripk1*$^{fl/fl}$) group and the red spots represent the up-regulated genes in *Ripk1*$^{\Delta hep}$ group. (E) The altered signaling pathways were enriched by KEGG analysis.